Generation of ultrashort laser pulses through a resonant interaction of quasi-continuous wave packet with running refractive index wave

I. O. Zolotovskii,[1,2,*] **D. A. Korobko,**[1] **V. A. Lapin,**[1] **P. P. Mironov,**[1] **D. I. Sementsov,**[1] **M. S. Yavtushenko,**[1] AND **A. A. Fotiadi**[1,3,4]

[1]*Ulyanovsk State University, 42 Leo Tolstoy Street, Ulyanovsk, 432970, Russian Federation*
[2]*National Research University of Electronic Technology—MIET, Bld. 1, Shokin Square, Zelenograd, Moscow, 124498, Russian Federation*
[3]*University of Mons, blvd. Dolez 31, Mons, B-7000, Belgium*
[4]*Ioffe Physical-Technical Institute, 26 Politekhnicheskaya, St Petersburg 194021, Russian Federation*
Corresponding author: rafzol.14@mail.ru

Modulation instability followed by generation of subpicosecond pulses could be obtained with quasi-continuous wave packets propagating in optical fibers with running refractive index wave. We report on comprehensive studies of this process demonstrating that the peak power of the pulses exceeds the power of the pumping radiation by orders of magnitude. Practically, the effect could be implemented through interaction of the surface optical wave with an acoustic wave in a 2 cm cylindrical waveguide in a robust all-fiber format. © 2019 Optical Society of America

1. INTRODUCTION

Fibers with running refractive index wave (RRIW) could enable effects never observed in the fibers with static index inhomogeneity or periodicity [1,2]. In particular, RRIW could provoke a switch of polarization and shift of carrier frequency of quasi-monochromatic wave packets [3–5]. Temporal pulse compression, a drastic increase of the pulse peak power accompanied by a decrease of the pulse duration, is a typical behavior for the pulses propagating in fibers with RRIW [1,2,5]. However, classical nonlinear effects, such as modulation instability, have not been studied comprehensively in such fibers yet [6–12].

Amplitude instabilities of CW radiation arising during its propagation in nonlinear media due to a cooperative action of nonlinear and dispersive effects support formation of localized waves [6] are referred to as modulation instabilities (MIs). The fundamental nature of the effect and its practical application for control of the laser radiation are both of great interest [11–16]. In particular, new designs of the laser systems delivering trains of picosecond and subpicosecond pulses with terahertz repetitive rate are of great demand for optical communication and metrology [17–24].

In this paper, we report on generation of subpicosecond pulse trains achieved through MI in optical fibers comprising running refractive index wave. Importantly, the generated pulses can reach the peak power by several orders of magnitude exceeding

the power of the pumping radiation. We propose a scheme enabling synchronization of a wave packet propagating as a surface tunneling wave (similar to whispering gallery mode) and RRIW generated in a waveguide by their velocities.

2. BASIC EQUATIONS

Let us consider an interaction of the frequency-modulated Gaussian pulse $A(t, z)$ with RRIW $n(t, z)$ induced in the fiber. The refractive index is described as

$$n(t, z) = n_0[1 - m\cos(\Omega t - qz)], \tag{1}$$

where Ω is the modulation frequency, $q = 2\pi/\Lambda$ is the wavenumber, Λ is the wave period, $m = \Delta n/n_0$ is the modulation depth, and Δn is the RRIW amplitude. The RRIW propagation velocity is $v_m = \Omega/q$. The co-propagating Gaussian pulse is introduced into the fiber with the following initial conditions:

$$A(t, z = 0) = A_0\exp(-(\tau_0^{-2} + i\alpha_0)t^2/2), \tag{2}$$

where A_0, τ_0, and α_0 are the pulse peak amplitude, pulse duration, and chirp, respectively, at the fiber input.

In the case when the light wave packet propagates synchronously with RRIW (their group velocities are equal), the envelope evolution is described as

$$\frac{\partial A}{\partial z} + v_g^{-1}\frac{\partial A}{\partial t} - i\frac{d_2}{2}\frac{\partial^2 A}{\partial t^2} + \frac{d_3}{6}\frac{\partial^3 A}{\partial t^3}$$

$$+ iR\left(|A|^2 - \tau_R\frac{\partial|A|^2}{\partial \tau}\right)A = i\Delta\beta A, \tag{3}$$

where $v_g = (\partial\omega/\partial\beta)_{\omega_0}$ is the wave packet group velocity, $d_n = (\partial^n\beta/\partial\omega^n)_{\omega_0}$ are high-order dispersion parameters for $n = 2, 3$, R is the cubic (Kerr) nonlinearity coefficient, the quantity

$$\Delta\beta = n_0 k_0 m \cos(\Omega t - qz) \tag{4}$$

is a change of the optical mode propagation constant in the fiber caused by modulation of the refractive index, $k_0 = \omega/c$, and τ_R is the Raman time constant [6].

In the running time frame ($\tau = t - z/v_g$), Eq. (3) has the form

$$\frac{\partial A}{\partial z} - i\frac{d_2}{2}\frac{\partial^2 A}{\partial\tau^2} + \frac{d_3}{6}\frac{\partial^3 A}{\partial\tau^3} + iR|A|^2$$

$$A = i\beta m \cos[\Omega(\tau - \delta\tau)]A, \tag{5}$$

where $\beta = n_0\omega/c$ is the wave packet propagation constant in the unexcited waveguide, c is the speed of light in a vacuum, and the quantity

$$\tau - \delta\tau = \tau - (v_m^{-1} - v_g^{-1})z$$

describes a relative delay of the pulse and RRIW. For pulses with sufficiently low delay ($\delta\tau \leq 10^{-11}$ s, at $|\Omega|\tau_p \ll 1$, where τ_p is the pulse duration) the right-hand side of Eq. (5) is approximated as

$$\cos[\Omega(\tau - \delta\tau)] \approx 1 - \Omega^2(\tau - \delta\tau)^2/2 \tag{6}$$

and Eq. (5) reduces to the Gross–Pitaevskii type equation (GPE) comprising high-order dispersion and nonlinear terms,

$$\frac{\partial A}{\partial z} - i\frac{d_2}{2}\frac{\partial^2 A}{\partial\tau^2} + \frac{d_3}{6}\frac{\partial^3 A}{\partial\tau^3} + iR\left(|A|^2 - \tau_R\frac{\partial|A|^2}{\partial\tau}\right)$$

$$A = i\left(S_1 + S_2\tau + S_3\tau^2\right)A, \tag{7}$$

with the parameters S_j:

$$S_1 = m\beta(1 - \Omega^2\delta\tau^2/2), \quad S_2 = m\beta\Omega^2\delta\tau, \quad S_3 = -m\beta\,\Omega^2/2.$$

Separating the variables z and τ, the amplitude of the wave packet envelope could be expressed as

$$A(z) = a(z)\exp\left[i(\varphi(z) + b(z)\tau + \alpha(z)\tau^2)\right]. \tag{8}$$

Substituting Eq. (8) into Eq. (7), we come to the equations for parameters:

$$\frac{\partial a}{\partial z} + d_2(b + 2\alpha\tau)\frac{\partial a}{\partial\tau} - i\frac{d_2}{2}\frac{\partial^2 a}{\partial\tau^2} + \frac{d_3}{6}\frac{\partial^3 a}{\partial\tau^3}$$

$$+ iR\left(|a|^2 - \tau_R\frac{\partial|a|^2}{\partial\tau}\right)a = \gamma(z)a, \tag{9a}$$

$$\frac{\partial b}{\partial z} + 2\alpha b d_2 = S_2, \tag{9b}$$

$$\frac{\partial\alpha}{\partial z} + 2d_2\alpha^2 = S_3, \tag{9c}$$

where

$$\gamma(z) = i\left(S_1 - \frac{\partial\varphi}{\partial z} - b^2 d_2 + i\alpha d_2\right),$$
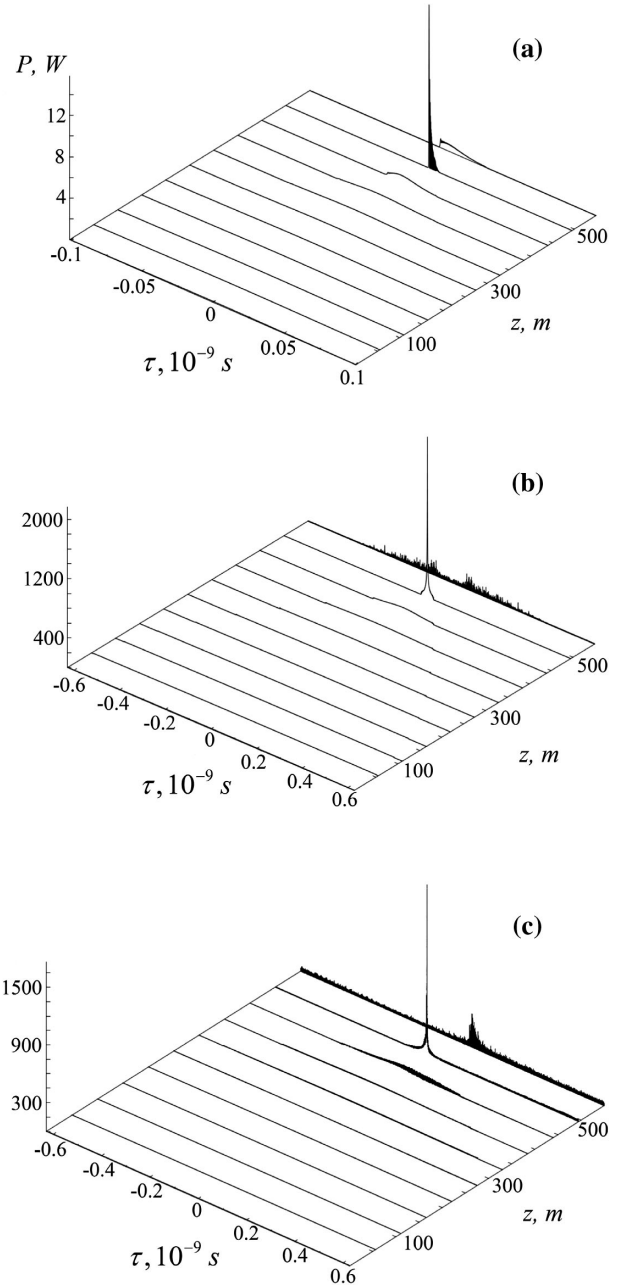
with

$$a = \bar{a}\exp[\gamma(z)dz]. \tag{10}$$

Fig. 1. (a) Quasi-linear and (b), (c) nonlinear dynamics of a Gaussian pulse simulated for the following parameters: (a) $\tau_p = 10^{-10}$ s, $P_0 = 0.1$ W, $d_2 = -10^{-26}$ s^2/m, $d_3 = 10^{-40}$ s^3/m, $R = 10^{-3}$ (W$\cdot$m)$^{-1}$; (b) $\tau_p = 10^{-9}$ s, $P_0 = 10$ W, $d_2 = -10^{-26}$ s^2/m $d_3 = 0$, $R = 10^{-3}$ (W$\cdot$m)$^{-1}$; (c) $\tau_p = 10^{-9}$ s, $\tau_R = 10^{-14}$ s, $P_0 = 10$ W, $d_2 = -10^{-26}$ s^2/m, $d_3 = 10^{-41}$ s^3/m, $R = 10^{-3}$ (W$\cdot$m)$^{-1}$, $\Omega = 10^9$ s^{-1}, $\beta = 10^7$ m^{-1}, $\Delta n = 10^{-4}$.

Equation (9a) is reduced to

$$\frac{\partial \bar{a}}{\partial z} + d_2(b + 2\alpha\tau)\frac{\partial \bar{a}}{\partial \tau} - i\frac{d_2}{2}\frac{\partial^2 \bar{a}}{\partial \tau^2} + \frac{d_3}{6}\frac{\partial^3 \bar{a}}{\partial \tau^3}$$

$$+ iR_{ef}\left(|\bar{a}|^2 - \tau_R\frac{\partial |\bar{a}|^2}{\partial \tau}\right)\bar{a} = 0, \qquad (11)$$
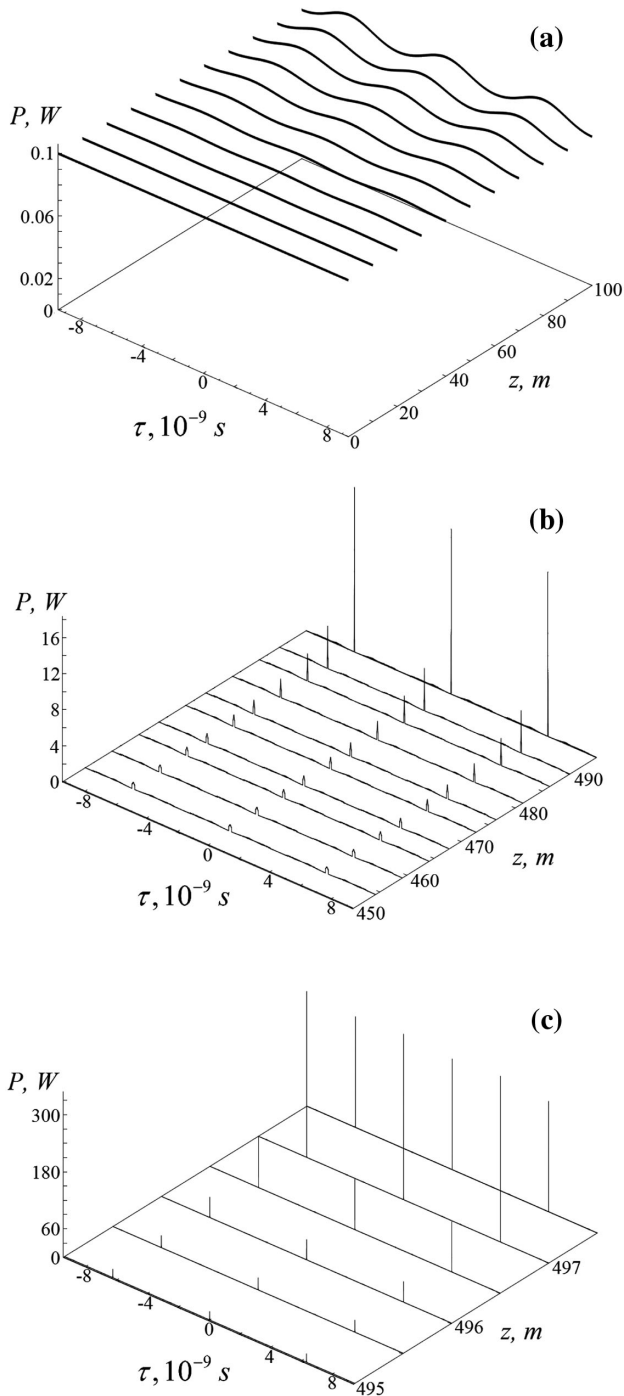
where $R_{ef} = f(z)R$ is the effective nonlinear coefficient.

For the case of anomalous dispersion considered further, the function $f(z)$ is

$$f(z) = \frac{1}{\cos(|\Omega|\sqrt{d_2 m\beta}z)}. \qquad (12)$$

An analysis of Eq. (9) shows that the fastest temporal compression and perturbation of the pulse (and other nonlinear processes) occur with the fiber length of
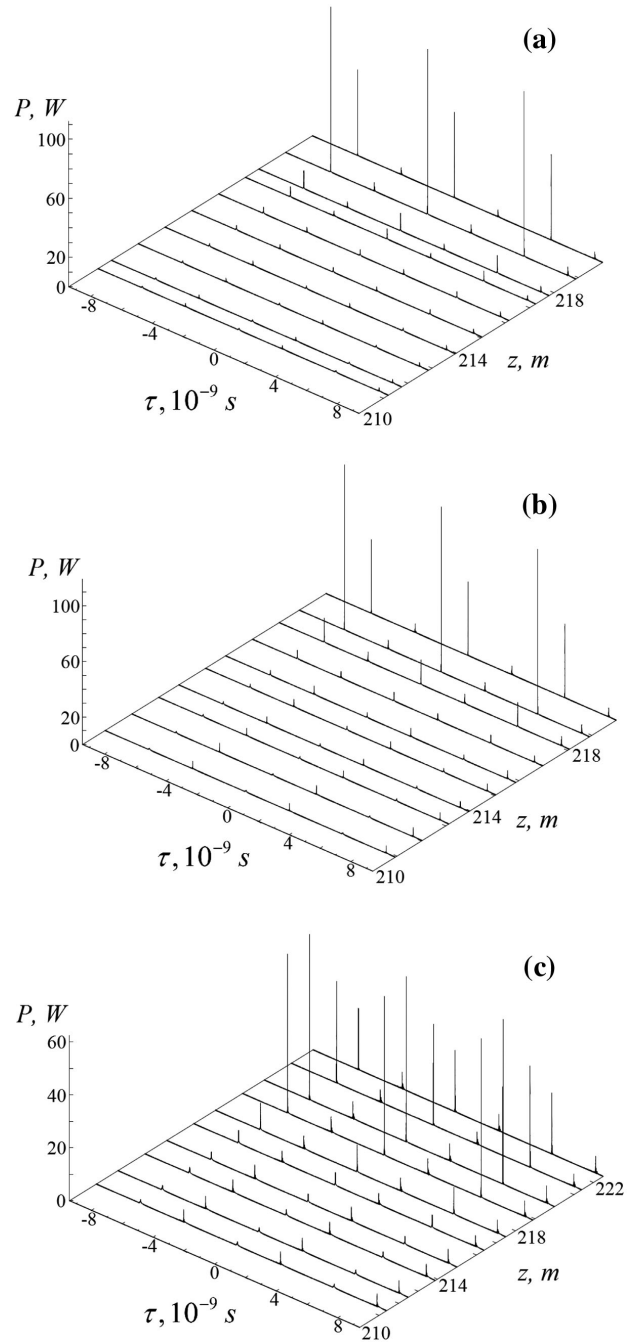

Fig. 2. (a)–(c) Transformation of a quasi-continuous wave into ultrashort pulse train for different waveguide lengths: $d_2 = -10^{-26}$ s²/m, $d_3 = 0$, $R = 10^{-3}$ (W·m)$^{-1}$, $P_0 = 0.1$ W, $\Omega = 10^9$ s^{-1}, $\beta = 10^7$ m^{-1}, $\Delta n = 10^{-4}$, $\Omega_{mod} = 10^{12}$ s^{-1}, $\zeta = 10^{-3}$, $\tau_R = 5 \cdot 10^{-15}$s.

Fig. 3. (a)–(c) Ultrashort pulse train generation at $d_2 = -10^{-26}$ s²/m $d_3 = 10^{-40}$ s³/m, $R = (10^{-3}, 10^{-2}, 10^{-1})$(W·m)$^{-1}$, $\tau_R = 5 \cdot 10^{-15}$ s; other parameters are the same as in Fig. 2.

$$z \to z_s = \frac{\pi}{2|\Omega|\sqrt{m\beta d_2}}. \tag{13}$$

Substituting the running time

$$\tau'(z) = f(z)\tau - d_2 \int f(z)b(z)dz, \tag{14}$$

Eq. (11) is reduced to

$$\frac{\partial \bar{a}}{\partial z} - i\frac{d_2^{ef}}{2}\frac{\partial^2 \bar{a}}{\partial \tau'^2} + \frac{d_3^{ef}}{6}\frac{\partial^3 \bar{a}}{\partial \tau'^3} + i R_{ef}|\bar{a}|^2\bar{a} = 0, \tag{15}$$

where $d_n^{ef}(z) = f^n(z)d_n(z)$ are the effective dispersion parameters. To reduce Eq. (7) to Eq. (15) we used the algorithm similar to so-called lens transformation [10,11]. Analysis of the derived equation shows that at $z \to z_s$, the function $f(z_s) \to \infty$, and the effective nonlinearity parameter $R_{ef}(z_s) \to \infty$. Therefore, a change of z_s should drastically change the wave packet behavior. In particular, at a very short length z_s, it experiences over-compression, i.e., $\tau_u(z_s) \to 0$, followed by ultrafast frequency and amplitude modulations, as shown in Figs. 1–3.

3. NUMERICAL ANALYSIS

Equation (5) differs from the well-known GPE by a parabolic potential Eq. (7) and is not singular. However, in the considered case, the numerical simulation demonstrates a strong compression of the pulse (by more than 2 orders of magnitude) followed by a sharp wave-breaking. Figure 1(a) presents evolution of a low-power Gaussian pulse described by Eq. (2) in the fiber with RRIW. The following fiber and pulse parameters have been used for simulation: $d_2 = -10^{-26}$ s²/m, $d_3 = 10^{-40}$ s³/m, $R = 10^{-3}$ (W·m)⁻¹, $P_0 = 0, 1$ W, $\Omega = 10^9$ s⁻¹, $\beta = 10^7$ m⁻¹, $\Delta n = 10^{-4}$ with the duration $\tau_p = 10^{-10}$ s. Numerical simulation of Eq. (7) has been performed by the split-step Fourier method (SSFM) with the variable step. The analytical solution [Eq. (12)] of Eq. (7) is used just to assist numerical simulation of Eq. (3). Indeed, Eq. (3) is a Gross–Pitaevskii type equation exhibiting a singularity near the point z_s. In the proximity to z_s the step of numerical calculation should be small enough to simulate the pulse evolution. Equation (12) allows estimation of the point z_s, advancing the simulations by the use of a step of 10 fs (i.e., 1 order of magnitude smaller than the narrowest pulse width) just in the proximity of z_s.

One can see that when the condition $|\Omega|\tau_p(0) \ll 1$ is satisfied, the pulse is compressed down to subpicosecond durations at the propagation length close to z_s demonstrating an increase of the peak pulse power by 3 orders of magnitude. One can see that with the used parameters (i.e., when nonlinear effects are low), Eq. (9) accurately describe the wave packet evolution and Eq. (13) determines the pulse compression length z_s with high precision.

In the case of a high-power pulse, its propagation over long fiber ($z > z_s$) is affected by high nonlinearity that causes pulse over-compression and breaking. Figure 1(b) shows evolution of a pulse of relatively long duration $\tau_{imp} = 10^{-9}$ s ($|\Omega|\tau_p(0) = 1$) over the fiber with $d_2 = -10^{-26}$ s²/m, $d_3 = 0$, $R = 10^{-3}$ (W·m)⁻¹, $P_0 = 10$ W, $\Omega = 10^9$ s⁻¹, $\beta = 10^7$ m⁻¹, $\Delta n = 10^{-4}$.

Figure 1(c) presents the dynamics of the superpulse formation under conditions similar to those used in Fig. 1(b), but with Raman self-scattering ($\tau_R = 10^{-14}$ s) and high value of the third-order dispersion $d_3 = 10^{-40}$ s³/m taken into account. Comparison of two evolutions highlight decrease of the superpulse amplitude, pulse shape deformation (with an appearance of right wing), and more earlier pulse distortion. Importantly, the pulse compression length z_s (≈ 500 m) does not change. One can see that at the propagation length close to z_s [≈ 500 m, Eq. (3)], the initial pulse experiences a strong compression down to the durations less than 1 ps along with an increase of the peak power up to the value higher than 1.5 kW (i.e., more than 2 orders of magnitude). However, at $z > z_m$, the wave packet breaks into separate noise components.

4. GENERATION OF SUPERPULSES

As shown above, when the velocities of RRIW and the wave packet are synchronized, ultrafast compression of the wave packet is possible. Therefore, it is reasonable to analyze evolution of MI in this case [7–17]. MI of the wave packet induced by an external parabolic potential [evolution of the wave packet is described by Eq. (7)] has been described neglecting the higher-order dispersion effects [10,11].

Numerical simulation of Eq. (5) has been performed by the SSFM [6] for quasi-continuous wave packet with a weak amplitude modulation:

$$A(0, \tau) = \sqrt{P_0}[1 + \zeta \cos(\Omega_{mod} \tau)], \tag{16}$$

where $P_0 = |A_0|^2$ is the input power, ζ is the modulation depth, and Ω_{mod} is the wave packet frequency modulation. Figure 2 presents evolution of MI and generation of ultrashort pulse train with the following simulation parameters: $d_2 = -10^{-26}$ s²/m, $d_3 = 0$, $R = 10^{-3}$ (W·m)⁻¹, $P_0 = 0.1$ W, $\Omega = 10^9$ s⁻¹, $\beta = 10^7$ m⁻¹, $\Delta n = 10^{-4}$, $\zeta = 10^{-3}$, $\Omega_{mod} = 10^{12}$ s⁻¹, and $\tau_R = 5 \cdot 10^{-15}$ s. The amplitude of the refractive index modulation used for simulations is quite realistic.

The scenario of superpulse generation [5,15,16] induced by MI is as the following. At the first stage shown in Fig. 2(a), the arising MI causes generation of high-frequency pulse train (breathers) with the repetition rate $\Omega_{max} = \sqrt{R_{ef} P_0/|d_{2ef}|}$ and duration of a single pulse $\tau_p \approx 2\pi/\Omega_{max}$. At this stage, the harmonic perturbation gain is expressed [6,15] as

$$g(z, \omega) = 2|\Delta\Omega d_{2ef}|\sqrt{2 R_{ef} P_0/|d_{2ef}| - \Delta\Omega^2}, \tag{17}$$

where $\Delta\Omega = \omega - \omega_0$, ω is the harmonic perturbation frequency, ω_0 is the carrier frequency of the input wave packet.

At the next stage, breathers are pulled toward the RRIW areas exhibiting the maximal refractive index, where a bunch of waves with an energy proportional to $W_s \sim P_0/\Omega$ are generated. An explosive character of subpicosecond pulse generation is clearly seen in the figure. For the continuous wave with a power of 100 mW (and the taken frequencies and modulation depths), the peak power of superpulses generated at the fiber length $z = z_m$ (that is of the same order of magnitude as z_s) is higher than $P_{max} > 0, 3$ kW. The resulting pulse duration is $\tau_s \sim P_0/\Omega P_{max}$ and shorter than a picosecond. With an

increase of the peak power, the repetition rate of the generated pulses decreases (for lower repetition rate, the energy generated by a superpulse increases due to additional energy of coherent breathers generated during time $T = 2\pi/\Omega$ and collapsed into a single superpulse). One can see that an ultrafast and sharp generation of subpicosecond pulses delivering kilowatt powers from a relatively low peak power pulse train occurs at the last stage, within the fiber length shorter than 1 m. Thus, a strong compression of the pulses induced by MI occurs at the final relatively short waveguide section.

Figures 2(b) and 2(c) highlight the dynamics of generation of the superpulse train. One can see a sharp increase of the superpulse peak power at $z \leq z_s$ caused by a coherent addition of the breathers generated through MI. Generation of high peak power ultrashort pulse occurs in the section short in comparison with the whole waveguide length. At $z > z_m$, light propagation becomes chaotic and finally the wave packet due to nonlinearity and higher-order dispersion effects breaks into noise components.

Figures 3(a)–3(c) show the dynamics of MI and generation of superpulse train from a continuous wave in fibers with RRIW. The third-order dispersion $d_3 = 10^{-40}$ s^3/m is taken now into account. The Kerr nonlinearities are $R = 10^{-3}, 10^{-2}, 10^{-1}$ (W·m)$^{-1}$ (a)–(c); all other parameters

are the same as in Fig. 2. The most efficient generation of ultrashort pulses is obtained at the optimal value of the nonlinearity $R \approx 10^{-2}$ (W·m)$^{-1}$. Noteworthy, at $R \leq 10^{-4}$ (W·m)$^{-1}$ no MI is observed.

Figures 4(a) and 4(b) present the shape that a superpulse acquires in the segment of maximal compression ($z \sim z_m$). The superpulse duration is approximately $\tau_{min} = 10^{-13}$ s. One should note that when the higher-order dispersion terms are negligible, the length of superpulse generation coincides with the length $z_s \approx z_m$ determined by Eq. (13) with high precision. As the Kerr nonlinearity increases by an order of magnitude (from $R = 10^{-3}$ (W·m)$^{-1}$ up to $R = 10^{-2}$ (W·m)$^{-1}$), the maximal superpulse peak power increases by about 10% (from about 110 up to 120) [Fig. 4(b)]. The shape of the pulse wings is nearly the same. Comparison of Figs. 4(a) and 4(b) highlights also the effect of the third-order dispersion. It is responsible for a break of the reflection symmetry, and therefore the pulse becomes slightly asymmetric, and the force pushing it off the resonance with the refractive index wave appears, decreasing the efficiency of the resonance interaction and the pulse amplitude.

For the pulse formation processes shown in Fig. 4, the effect of Raman scattering is negligible. Although the maximal peak pulse amplitude could be as high as ~ 400 W [Fig. 4(a)], the effective Raman amplification length (the length corresponding to the power increases in e times) is rather short (typically ~ 1 m). Therefore, with $\tau_R = 5 \cdot 10^{-15}$ s the Raman gain increment is estimated to be ~ 0.4 [Fig. 4(a)], which is much lower than ~ 16, i.e., the commonly accepted Raman threshold increment [6].

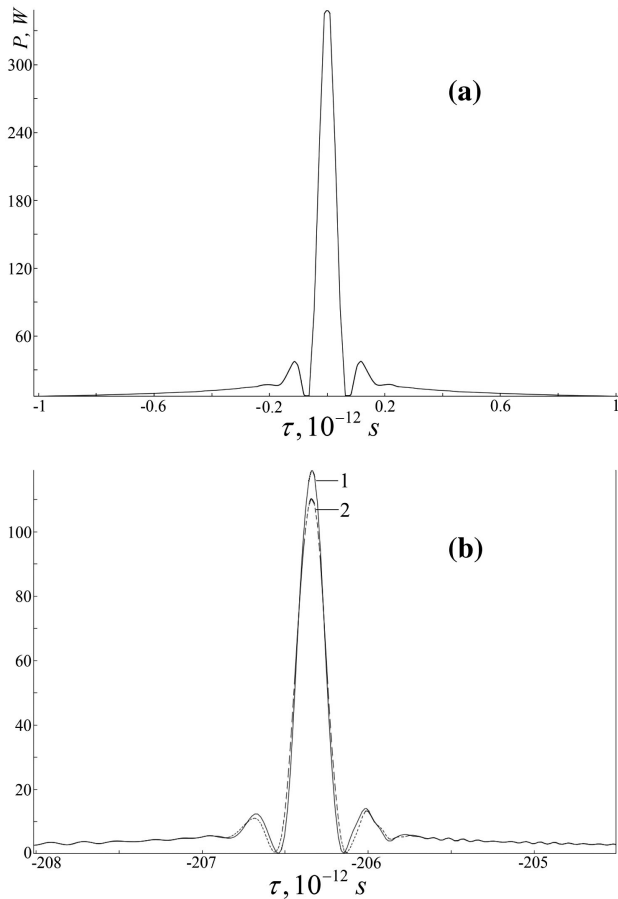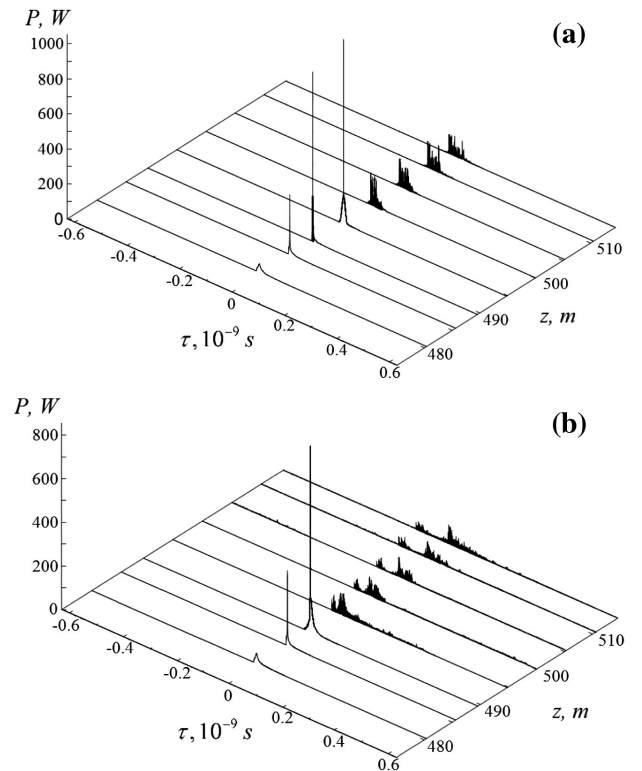**Fig. 4.** (a), (b) Temporal dependence of superpulse power simulated for the lengths $z \approx z_s = 497$ m: (a) $d_2 = -10^{-26}$ s^2/m, $P_0 = 0.1$ W, $\Omega = 10^9$ s^{-1}, $\beta = 10^7$ m^{-1}, $\Delta n = 10^{-4}$, $d_3 = 0$, $\tau_R = 510^{-15}$ s; (b) $d_3 = 10^{-40}$ s^3/m, $R = 10^{-2}, 10^{-3}$ (W·m)$^{-1}$, $\tau_R = 5 \cdot 10^{-15}$ s (1, solid line; 2, dashed line).

Fig. 5. (a), (b) Evolution of the superpulse formation: $P_0 = 1$ W, $d_2 = -10^{-26}$ s^2/m, $\Omega = 10^9$ s^{-1}, $\beta = 10^7$ m^{-1}, $\Delta n = 10^{-4}$, $d_3 = 10^{-41}$ s^3/m, $\varsigma = 10^{-3}$, $\Omega_{mod} = 10^{12}$ s^{-1}, $R = 10^{-3}$ (W·m)$^{-1}$; (a) $\tau_R = 5 \cdot 10^{-15}$ s; (b) $\tau_R = 5 \cdot 10^{-14}$ s.

To evaluate the effect of the Raman scattering on the super-pulse formation we have simulated the pulse formation dynamics at much higher input power of $P_0 = 1$ W. In this case the superpulse amplitude gets ~ 1 kW and the Raman effect becomes important. Figure 5 compares dynamics of the pulse formation for two different values of the Raman response time τ_R. One can see that after getting the Raman threshold the Raman effect suppresses the pulse peak amplitude, leading to the pulse distortion. In addition, the Raman effect shortens the compression lengths, which become ~ 496 and ~ 489 m for $\tau_R = 5 \cdot 10^{-15}$ s and $\tau_R = 5 \cdot 10^{-14}$ s, respectively. From comparison of Figs. 4 and 5 one can see that at higher peak power levels the effect of the third-order dispersion is more pronounced. In Fig. 5 the pulse exhibits asymmetric deformation typical for the third-order dispersion effect.

5. PRACTICAL IMPLEMENTATION OF THE SIMULATED EFFECT

Considering the dynamics of a pulse or quasi-continuous wave packet in a fiber with RRIW, we have assumed an equality of their velocities ($v_g \approx v_m = \Omega/q$). These conditions could be implemented in the real waveguide through interaction of RRIW and surface wave (similar to whispering gallery mode), the so-called tunneling wave [25,26]. In this configuration, the wave packets propagate in a spiral along the surface of a silica cylindrical waveguide with a constant helix step. The longitudinal (along the waveguide axis) group velocity is less than the speed of light propagating along the waveguide and could be adjusted to the RRIW velocity by a selection of the angle of the light injection [26–29].

When the light is injected into a cylindrical waveguide at a certain angle to the cylinder axe, the surface wave propagates along a spiral trajectory (Fig. 6) [25,26,28–30]. For this wave, the longitudinal component of the wave vector is $k_z = (k^2 - k_r^2)^{1/2}$, where $k = k_0 n(\omega)$; $k_0 = \omega/c$ is the wavenumber in vacuum; $n(\omega)$ is the refractive index of the waveguide material; and k_r is the transverse (radial) wave vector component. When the angle of the wave injection into the fiber is close to the normal, the wave propagation along the waveguide slows down significantly. The surface wave slowly propagates along the longitudinal axis of the waveguide z with velocity $V_c \ll c$ (when $k_z \ll k \sim k_r$). The wave electric field in this case can be expressed as

$$E(z, r, t, \varphi) = A(z, t)\Phi(r, z, \varphi) \exp\left(i\omega t - i\int_0^z k_z(z)\mathrm{d}z\right),$$
(18)

where $A(z, t)$ is the slowly varying amplitude describing the longitudinal (along the z axis) distribution of the tunneling wave field, and $\Phi(r, z, \varphi)$ is the function determining the radial and azimuthal dependence of the field inside the waveguide (at $r \leq a_0$, where a_0 is the fiber radius) [1,29].

The dynamics of a wave packet temporal envelope is described by the nonlinear Schrödinger equation [20]:

$$\frac{\partial A}{\partial \xi} - i\frac{d_2}{2}\frac{\partial^2 A}{\partial \tau^2} + \frac{d_3}{6}\frac{\partial^3 A}{\partial \tau^3}$$
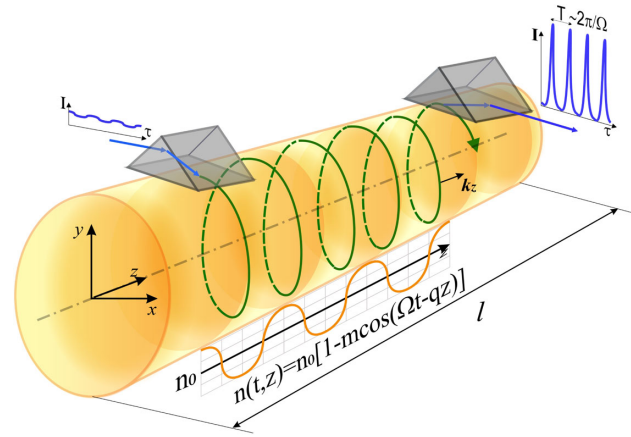$$+ i R_m |A|^2 A = i\beta m \cos[\Omega(\tau - \delta\tau)]A.$$
(19)

Fig. 6. Propagation of the tunneling wave synchronized with RRIW over the cylinder surface.

This equation is similar to Eq. (5), but with ξ coordinate along the wave packet trajectory used instead of z coordinate along the waveguide. Therefore, ξ is related to z as follows:

$$\partial\xi \simeq (v_g/v_m)\partial z \simeq (c/nv_m)\partial z \simeq \gamma^{-1}\partial z,$$

where $\gamma \simeq nv_m/c$ is the wave deceleration parameter, $R_m = kn^{(2)}/S_{ef}$ is the nonlinearity parameter, $n^{(2)}$ is the cubic nonlinearity coefficient of material, and S_{ef} is the effective area of the surface tunneling mode [6,29].

Such an interaction of the wave packet and RRIW could be achieved in the fiber with an induced acoustic wave [28–31]. To synchronize the tunneling wave packet and RRIW in silica fiber with a standard refractive index $n \approx 1.5$ and the acoustic wave velocity $V_a \approx \gamma c/n \approx 6000$ m/s, the Kerr nonlinearity $\gamma \approx 3 \cdot 10^{-5}$ is required. The modulation depth m provided by the acoustic wave can be as high as $m = 4 \cdot 10^{-4}$ [1,31]. In this case, a cylindrical waveguide with the length l of 2 cm only (for which $\xi = l/\gamma \approx 500$ m) enables a surface tunneling wave induced by MI leading to generation of a train of pulses with the peak power several orders of magnitude greater than that of the pumping radiation.

6. CONCLUSION

In this paper, we report on the nonlinear dynamics of a wave packet propagating in a waveguide with RRIW. The regimes of MI in such fibers are explored. We have shown that subpicosecond pulses generated through MI could acquire the peak powers by orders of magnitude higher than the power of CW pumping radiation. Practical realization of the effect could enable a compact (shorter than 1 cm) all-fiber generator of picosecond and subpicosecond pulse trains. It is worth noting that the reported MI significantly defers from that commonly observed in optical fibers (including nonhomogeneous fibers) [22–24]. Equation (7), used for describing dynamics of the Bose–Einstein condensate (BEC) [32–35] and, therefore, formation dynamics of the gigantic pulses described here, is similar to BEC wave dynamics reported early for the magnetic trap with parabolic potential near Feshbach resonance.

REFERENCES

1. V. P. Torchigin, "Possibility of using the interaction of acoustic and light waves in optical fibers to generate short light pulses," Quantum Electron. **23**, 235–240 (1993).
2. V. P. Torchigin, "Amplification of light pulses in waveguides with a periodically varying refractive index," Quantum Electron. **25**, 484–485 (1995).
3. V. P. Torchigin, "Possibility of generating coherent light via microwave modulation of the index of refraction of an optical fiber," Quantum Electron. **23**, 241–246 (1993).
4. A. N. Buliuk, "Electro-optic modulation and frequency translation of light in a gyrotropic medium," Quantum Electron. **25**, 66–70 (1995).
5. I. O. Zolotovskii, V. A. Lapin, and D. I. Sementsov, "Frequency modulation and compression of optical pulses in an optical fibre with a travelling refractive-index wave," Quantum Electron. **46**, 39–44 (2016).
6. G. Agrawal, *Nonlinear Fiber Optics*, 4th ed. (Springer, 2007).
7. V. E. Zakharov and L. A. Ostrovsky, "Modulation instability: the beginning," Phys. D **238**, 540–548 (2009).
8. K. Tai, A. Hasegawa, and A. Tomita, "A historical narrative of study of fiber grating solitons," Phys. Rev. Lett. **56**, 135–138 (1986).
9. E. M. Dianov, P. V. Mamyshev, A. M. Prokhorov, and S. V. Chernikov, "Generation of a train of fundamental solitons at a high repetition rate in optical fibers," Opt. Lett. **14**, 1008–1010 (1989).
10. V. V. Konotop and M. Salerno, "Modulational instability in Bose-Einstein condensates in optical lattices," Phys. Rev. **A65**, 021602 (2002).
11. B. B. Baizakov, V. V. Konotop, and M. Salerno, "Regular spatial structures in arrays of Bose-Einstein condensates induced by modulational instability," J. Phys. B **35**, 5105 (2002).
12. A. M. Rubenchik, S. K. Turitsyn, and M. P. Fedoruk, "Modulation instability in high power laser amplifiers," Opt. Express **18**, 1380–1388 (2010).
13. D. A. Korobko, O. G. Okhotnikov, and I. O. Zolotovskii, "High-repetition-rate pulse generation and compression in dispersion decreasing fibers," J. Opt. Soc. Am. B **30**, 2377–2386 (2013).
14. Q. Li, K. Nakkeeran, and P. K. A. Wai, "Ultrashort pulse train generation using nonlinear optical fibers with exponentially decreasing dispersion," J. Opt. Soc. Am. B **31**, 1786–1792 (2014).
15. D. A. Korobko, S. G. Moiseev, and I. O. Zolotovskii, "Induced modulation instability of surface plasmon polaritons," Opt. Lett. **40**, 4619–4622 (2015).
16. T. Tanemura and K. Kikuchi, "Unified analysis of modulational instability induced by cross-phase modulation in optical fibers," J. Opt. Soc. Am. B **20**, 2502–2514 (2003).
17. P. Franco, F. Fontana, I. Cristiani, M. Midrio, and M. Romagnoli, "Self-induced modulational-instability laser," Opt. Lett. **20**, 2009–2011 (1995).
18. E. Yoshida and M. Nakazawa, "Low-threshold 115-GHz continuous-wave modulational-instability erbium-doped fiber laser," Opt. Lett. **22**, 1409–1411 (1997).
19. Y.-X. Zhang, X.-Y. Pu, K. Zhu, and L. Feng, "Threshold property of whispering-gallery-mode fiber lasers pumped by evanescent waves," J. Opt. Soc. Am. B **28**, 2048–2056 (2011).
20. I. O. Zolotovskii, D. A. Korobko, V. A. Lapin, and D. I. Sementsov, "Modulation instability of pulsed radiation in an optical waveguide in the presence of the traveling refractive index wave," Opt. Spectrosc. **121**, 256–262 (2016).
21. A. W. Snyder and J. Love, *Optical Waveguide Theory* (Springer, 1983).
22. A. Mussot, M. Conforti, S. Trillo, F. Copie, and A. Kudlinski, "Modulation instability in dispersion oscillating fibers," Adv. Opt. Photonics **10**, 1–42 (2018).
23. N. Tarasov, A. M. Perego, D. V. Churkin, K. Staliunas, and S. K. Turitsyn, "Mode-locking via dissipative Faraday instability," Nat. Commun. **7**, 12441 (2016).
24. A. M. Perego, N. Tarasov, D. V. Churkin, S. K. Turitsyn, and K. Staliunas, "Pattern generation by dissipative parametric instability," Phys. Rev. Lett. **116**, 028701 (2016).
25. O. V. Ivanov, S. A. Nikitov, and Y. V. Gulyaev, "Cladding modes of optical fibers: properties and applications," UFN **176**, 175–202 (2006).
26. V. A. Sychugov, L. N. Magdich, and V. P. Torchigin, "Interaction of whispering-gallery electromagnetic waves with acoustic waves in tapered quartz rods," Quantum Electron. **31**, 1089–1094 (2001).
27. V. A. Sychugov, V. P. Torchigin, and M. Y. Tsvetkov, "Whispering-gallery waves in optical fibres," Quantum Electron. **32**, 738–742 (2002).
28. V. P. Torchigin and S. V. Torchigin, "Optical solitons appearing during propagation of whispering-gallery waves," Quantum Electron. **33**, 913–918 (2003).
29. M. Sumetsky, "Whispering-gallery-bottle microcavities: the three-dimensional etalon," Opt. Lett. **29**, 8–10 (2004).
30. S. V. Suchkov, M. Sumetsky, and A. A. Sukhorukov, "Reflectionless potentials for slow whispering gallery modes in surface nanoscale axial photonic fiber resonators," Opt. Lett. **40**, 3806–3809 (2015).
31. A. P. Goutzoulis and D. R. Pape, *Design and Fabrication of Acousto-Optic Devices* (Marcel Dekker, 1994).
32. K. Staliunas, S. Longhi, and G. J. de Valcarcel, "Faraday patterns in Bose-Einstein condensates," Phys. Rev. Lett. **89**, 210406 (2002).
33. K. Staliunas, S. Longhi, and G. J. de Valcarcel, "Faraday patterns in low-dimensional Bose-Einstein condensates," Phys. Rev. A **70**, 011601 (2004).
34. Y. S. Kivshar, T. J. Alexander, and S. K. Turitsyn, "Nonlinear modes of a macroscopic quantum oscillator," Phys. Lett. A **278**, 225–230 (2001).
35. B. A. Malomed, *Soliton Management in Periodic Systems* (Springer, 2006).